Journal of Materials Chemistry C

PAPER

View Article Online
View Journal | View Issue

Cite this: J. Mater. Chem. C, 2017, 5, 8444

Highly transparent polyhydroxyimide/TiO_2 and ZrO_2 hybrid films with high glass transition temperature (T_g) and low coefficient of thermal expansion (CTE) for optoelectronic application†

Shun-Wen Cheng,‡ Tzu-Tien Huang,‡ Chia-Liang Tsai and Guey-Sheng Liou *

Received 24th June 2017,
Accepted 19th July 2017

DOI: 10.1039/c7tc02819a

rsc.li/materials-c

A novel polyhydroxyimide and the respective polymer hybrids of titania or zirconia with remarkable thermal stability and optical properties have been successfully prepared. Polyhydroxyimides (**PHIs**) with high transparency were synthesized through one-step polycondensation. The hydroxyl groups in the repeating units of polymer backbone contribute organic–inorganic bonding reaction sites for preparing homogeneous films of hybrids. The hybrids displayed low coefficient of thermal expansion (CTE) (23 ppm $^{\circ}C^{-1}$ for **PHI-BCZr30**) and extraordinary thermal stability essential to sustain high glass transition temperatures (T_g) (350–410 °C). The transparency of thin film based on **PHI-BC** reaches 96% at 400 nm, and the refractive index of **PHI-6F** reaches 1.63. In addition, these polymer films of the hybrids revealed tunable refractive index (1.63–1.84 for **PHI-6F/TiO_2** and 1.63–1.81 for **PHI-6F/ZrO_2**), and the hybrid films of **PHI-BC/ZrO_2** exhibited higher Abbe's number and optical transparency than those of **PHI-BC/titania** system because of a larger band gap of zirconia. On introducing titania and zirconia, as electron acceptors, into **PHI-6F**, the charge-transfer complex could be facilitated and stabilized owing to the lower LUMO energy level of the resulting materials of the hybrid. Consequently, the memory devices fabricated from the polymer hybrid films manifested tunable memory properties from SRAM, and DRAM, to WORM at various titania or zirconia contents from 0 to 50 wt% with a high ON/OFF ratio (10^8). Moreover, various energy levels of titania and zirconia demonstrated the uniquely distinct memory characteristics, indicating that the **PHIs/TiO_2** and **PHIs/ZrO_2** hybrid films, as memory devices with high transparency, have strong potential in electrical applications.

Introduction

Polymer–inorganic hybrid materials combine plentiful advantages of inorganic materials and organic polymers, such as outstanding optical, electric and mechanical properties and thermal stability and processability, and draw a lot of attention for optoelectronic applications.[1] After a brief introduction of the basic methodology for developing polymers of high refractive index (RI; n) with important parameters including Abbe's number (V_d) and birefringence (Δn), some of their applications such as antirefractive coatings, microlenses for CMOS image sensors and encapsulants for LEDs are highlighted.[2,3]

For the polymer matrix, conventional polyimides (PIs) like Kapton produced by DuPont have been applied to aerospace fields and microelectronic devices. Notwithstanding, the yellow colour of aromatic polyimide is a critical disadvantage that made it difficult to be used in optoelectronics due to the intramolecular or intermolecular charge-transfer complex (CTC) formation between the diamines (electron-donating groups) and the aromatic dianhydrides (electron-accepting groups). Thus, the highly transparent polyimides are necessary and can be obtained by modifying the molecular structure through the introduction of fluoroalkyl and alicyclic groups, which isolated linkages to suppress the interactions between colour-causing moieties.[4]

For the hybrid system, how to make a judicious choice of inorganic materials is a crucial issue for enhancing RI and V_d without sacrificing optical transparency in the visible light region.[5] In our previous studies,[6,7] the PI/titania hybrids showed higher refractive index and thermal stability with the increasing TiO_2 content. However, the transparency of the hybrids reduced dramatically at 400 nm, and Abbe's number of PI/titania films of the hybrid also reduced when the TiO_2 content increased. Thus, in order to obtain PI hybrids with higher transparency in the visible region, it is inevitable to utilize inorganic materials with larger band gap like ZrO_2.[6f] The resulting PI/ZrO_2 films of the hybrid demonstrated much

Institute of Polymer Science and Engineering, National Taiwan University, Taipei, 10617, Taiwan. E-mail: gsliou@ntu.edu.tw

† Electronic supplementary information (ESI) available: ^{1}H NMR spectra, IR spectra, UV-visible absorption spectra, thermal properties, retention times and cyclic voltammetric diagrams of the hybrid materials. See DOI: 10.1039/c7tc02819a

‡ The authors contributed equally to the work.

higher transparency in the visible light region owing to the ZrO_2 (5.0–5.85 eV) having a larger energy band gap than TiO_2 (3.2 eV). Moreover, the main requirement is that the domain size of inorganic materials should be smaller than 40 nm for obtaining transparent nanocomposites.[8] For optical materials, a further reduction in the diameter of filler particles is essential for less loss of scattering and maintenance of optical transparency of the pristine polymer matrixes. To avoid agglomeration, the *in situ* sol–gel hybridization method is a facile approach that restricts the organic–inorganic material interactions at the interface, and the domain size of the inorganic particles can be controlled to a level around 5 nm.[6]

In addition to the optical applications, recently, hybrids of the polymer have also attracted much attention in the development of memory devices. With the introduction of additional metal nanoparticles and organic electron-donor and -acceptor molecules into the polymers, the formation of charge-transfer (CT) complex can be further improved.[9] Recently, we have also attempted to introduce the PCBM or TiO_2[10] into the polyimide system. These nanoparticles can act as strong electron acceptors owing to the lower LUMO energy level, which stabilizes and facilitates the CT effect. The incorporation of TiO_2 or ZrO_2 avoids the drawback of reducing ON/OFF ratios at high TiO_2 or ZrO_2 content because the conductivity is still low for TiO_2 and ZrO_2 in the OFF state. For polymer hybrids, the mechanism to operate memory behaviour can be ascribed to the CT effect, and the thickness should always be controlled within 100 nm. Therefore, it is a prerequisite for nano-scale memory devices that the domain size of inorganic particles should be extremely small and well dispersed in polymer matrix.

In this study, we synthesized the highly transparent and flexible polyhydroxyimide (PHI) with hydroxyl groups in the repeating units of PHI, which contributed organic–inorganic sites of bonding. The corresponding **PHIs/TiO_2** and **ZrO_2** hybrid films were also prepared, for investigating optical properties such as transparency, refractive Index and Abbe's number, and electrical memory behaviour of memory devices stemmed from the PI hybrid films.

Experimental

Synthesis of 4,4′-diamino-4″-hydroxytriphenylmethane (DHTM)[11]

The general synthetic route for preparing **PHIs** is shown in Scheme 1. More details can be found in the ESI.†

Preparation of polyhydroxyimides (PHIs)

The general synthetic route for preparing **PHI** is depicted in Scheme 2. The inherent viscosity, average molecular weight and solubility behaviour of prepared **PHIs** are summed up in Table 1. More details can be found in the ESI.†

Preparation of the PHI films

The DMAc solution of **PHI** was casted onto a glass substrate, and the solvent was removed under vacuum at 80 °C for 6 h and 150 °C for 8 h to obtain polymer films with thicknesses of about 20 μm that were applied for optical and thermal measurements, and solubility tests.

Preparation of PHIs/titania and PHIs/zirconia hybrid films

Scheme 3 depicts the procedure for preparing the hybrid films of **PHIs**/titania (**PHIsTiX**). More details can be found in the ESI.†

Results and discussion

Synthesis of 4,4′-diamino-4″-hydroxytriphenylmethane (DHTM)

According to the reference paper,[11] the diamine containing the hydroxyl group **DHTM**, was prepared by the reaction of

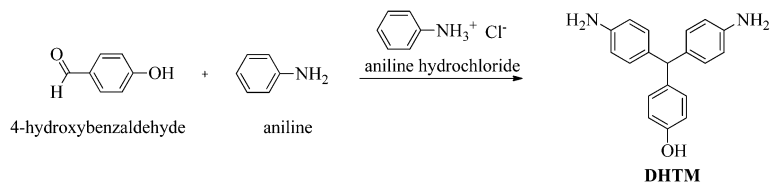

Scheme 1 Preparation of 4,4′-diamino-4″-hydroxytriphenylmethane (**DHTM**).

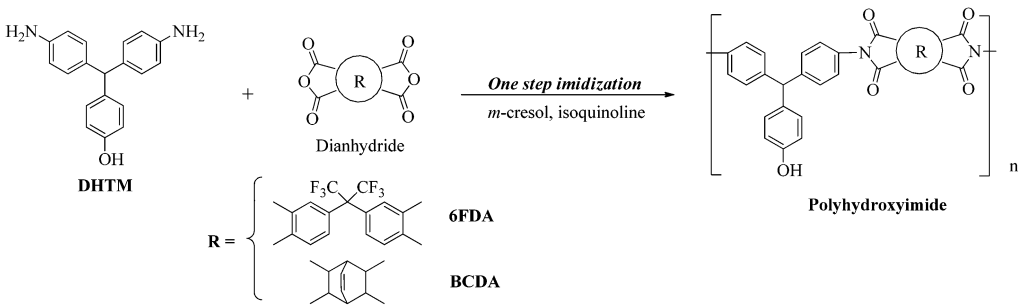

Scheme 2 Preparation of polyhydroxyimides (**PHIs**).

Table 1 Inherent viscosity, GPC data and solubility behavior of **PHIs**

Polymer	η^a (dL g^{-1})	GPC data[b]			Solubility in different solvents[d]						
		M_n	M_w	PDI[c]	DMAc	DMSO	NMP	DMF	*m*-Cresol	THF	$CHCl_3$
PHI-6F	0.72	66 000	84 000	1.26	++	++	++	++	+−	++	+−
PHI-BC	0.39	25 000	35 000	1.39	++	++	++	++	++	−−	−−

[a] Measured at 0.5 g dL^{-1} polymer concentration in DMAc at 30 °C. [b] Calibrated with polystyrene standards at a constant flow rate of 0.5 mL min^{-1} at 40 °C (eluent: NMP). [c] Polydispersity index (M_w/M_n). [d] The solubility was determined by using 2 mg of sample in 2 mL of solvent. ++: soluble at room temperature; +: soluble on heating; +−: partially soluble or swell on heating; −: insoluble even on heating.

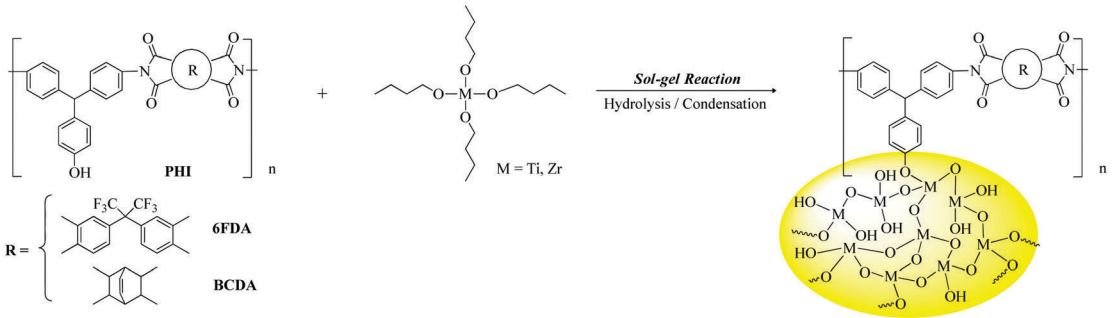

Scheme 3 Preparation and structure of **PHIs/TiO_2** and **PHIs/ZrO_2** hybrid.

4-hydroxybenzaldehyde with excess aniline in the presence of aniline hydrochloride, as shown in Scheme 1. The obtained **DHTM** was purified by vacuum sublimation to yield a crystalline product that appears as purple needles. The yield was 25.39 g (48%): Mp = 200–202 °C. ^{1}H NMR (DMSO-d_6): 9.1 (s, OH, 1H), 6.9–6.4 (m, PhH, 12H), 5.0 (s, CH, 1H) and 4.8 (s, NH2, 4H) (Fig. S1 (ESI†)).

Polymer synthesis and characterization

The hydroxyl-containing polyimides **PHIs**, were prepared from **DHTM** with 6FDA or BCDA in *m*-cresol. First, poly(amic acid), which is a precursor of the polyimide, was produced and dehydrated to PI with the supplement of isoquinoline at 170–180 °C for 15 h (Scheme 2). Then, when this resulting PI solution was slowly poured into a mixture of water and methanol, the **PHIs** were obtained in a white fibre-like form. The **DHTM** used in this study contained triphenylmethane that effectively suppressed the electronic interaction between color-causing moieties.[4] Moreover, the fluoroalkyl- and alicyclic-containing dianhydrides also increased the transparency of the obtained PIs by lowering the charge-transfer (CT) interactions. The inherent viscosity, solubility behaviour and average molecular weight of the resulting **PHIs** are summarized in Table 1. These PIs dissolve in DMF, DMSO, DMAc, and NMP solvents and can also be casted as solution into transparent and flexible films, as shown in Fig. 1a and d. FT-IR spectra of **PHI** films depicted in Fig. S2 (ESI†) show absorption bands in the range from 3000 to 3750 cm^{-1} (carboxylic acid O–H stretch): for imide, 1780 cm^{-1} (asymmetrical C═O) and 1725 cm^{-1} (symmetrical C═O), 1375 cm^{-1} (C–N), and 734 cm^{-1} (deformation of the imide ring).

Preparation and characterization of PI hybrids

The sol–gel reaction of **PHI-6F** with **TiO_2** and **ZrO_2** precursors was applied to prepare **PHI-6F/TiO_2** and **PHI-6F/ZrO_2** (**PHI-6FMX**) films depicted in Scheme 3. Formations of transparent optical hybrid films illustrated in Fig. 1 demonstrate that the hydroxyl groups in **PHI-6F** contribute the reaction sites for the bonding between organic and inorganic materials. The FT-IR spectra of **PHI-6FTi30** and **PHI-6FZr30** hybrid films, shown in Fig. S3 (ESI†), display absorption bands in the range from 3000 to 3700 cm^{-1} (O–H stretch) with a larger intensity of signal than that of the pristine **PHI-6F** owing to the newly formed hydroxyl groups in the TiO_2 and ZrO_2. Moreover, the inorganic absorption bands of Ti–O–Ti and Zr–O–Zr at 650–800 and 600–650 cm^{-1}, respectively, can be observed.[6,7]

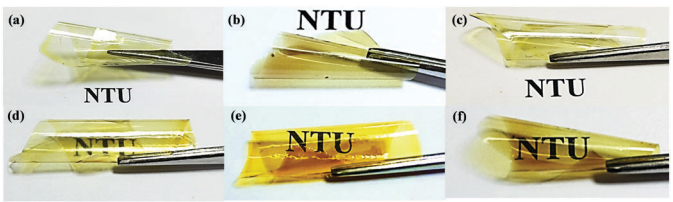

Fig. 1 Transparent and flexible optical films: (a) **PHI-BC**, (b) **PHI-BCTi30**, (c) **PHI-BCZr30**, (d) **PHI-6F**, (e) **PHI-6FTi30** and (f) **PHI-6FZr30** (thickness: 20 ± 5 μm).

Thermal properties of PHIs, PHIs/TiO_2 and PHIs/ZrO_2

The thermal properties of the **PHI**, **PHI-6F/TiO_2** and **PHI-6F/ZrO_2** films of hybrid (**PHI-6FMX**) were measured by thermogravimetric analysis (TGA) and thermal mechanical analysis (TMA). The results are summed up in Table 2. By TGA measurement, the resulting PI hybrid materials showed excellent thermal stability both in air and nitrogen, and the increasing char yield can be attributed to the enhancement of inorganic material contents as displayed in Fig. S4 (ESI†). In addition, for these hybrid systems, the char yield under flow of air can be used to confirm the content of inorganic materials, and the results were in good agreement with the theoretical values, which also confirmed the incorporation of inorganic nanoparticles successfully. The TMA measurements of pristine **PHI-6F** exhibited the T_g up to 350 °C, which could be promoted to 400 °C and 410 °C at the contents of 30 wt% TiO_2 and ZrO_2, respectively, as shown in Fig. S5 (ESI†). Furthermore, the values of an important reference parameter in the microelectronic applications called the coefficient of thermal expansion (CTE) for these polymer films are also summarized in Table 2.

Organic matrixes usually have much higher CTE value than inorganic reinforced materials. Thus, the resulting hybrid films effectively suppress CTE when the volume fraction of inorganic nanoparticles is increased. It is worth to mention that the CTE value can be reduced to 23 and 25 at 30 wt% content of **ZrO_2** with T_g up to 355 °C and 410 °C in **PHI-BC** and **PHI-6F**, respectively.

Optical properties of PIs and hybrid films

The UV-vis transmission spectra of **PHIs**, **PHIs/TiO_2** and **PHIs/ZrO_2** hybrid thin and thick films with thickness of 200–300 nm and 20 ± 3 μm, respectively, were measured as summed up in Fig. 2 and Table 3. The **PHI** films prepared from fluoroalkyl- and alicyclic-containing dianhydrides revealed remarkable optical transparency and refractive index; the transparency of **PHI-BC** thin films was extremely high up to 96% at 400 nm, and the refractive index of **PHI-6F** could reach 1.63. Nonetheless, the optical transparency of the corresponding hybrid films of **PHI-6F/TiO_2** and **PHI-BC/TiO_2** decreased apparently at 400 nm due to the low band gap of TiO_2 (3.2 eV), resulting in a pale yellow color of the hybrid films, for which the domain size of TiO_2 is smaller than 10 nm. In addition, when the amount of inorganic nanoparticles in the hybrid film increased, there was be a negligible variation in the particle size, which in turn enhanced the redshift phenomenon.[6] In contrast, the **PHI-6F/ZrO_2** and **PHI-BC/ZrO_2** films of hybrid demonstrated higher transparency in the region of visible light because zirconia has larger energy band gap (5.0 to 5.85 eV) than the respective **PHI-6F/TiO_2** and **PHI-BC/TiO_2** system. Furthermore, the TEM images of hybrid material **PHIs/ZrO_2** illustrated in Fig. 4 indicate that the ZrO_2 has good dispersion with a domain size smaller than 10 nm, resulting in lower cut-off wavelengths and excellent optical transparency of these **PHIs/ZrO_2** hybrid films in addition to larger energy band gap of zirconia.

The RI diagrams in the range of 300–800 nm of these hybrid films with different TiO_2 and ZrO_2 contents are summarized in Fig. 3, and the inset figures display the variety of RI at 633 nm; the RI increased with increasing amount of inorganic materials, implying that the inorganic precursors of Ti–OH or Zr–OH groups could successfully form structures of Ti–O–Ti and Zr–O–Zr by sol–gel reaction. In addition, Abbe's number (V_d; variation of RI *versus* wavelength) is a decisive parameter for optical materials that indicate lower optical dispersion for the materials with a high value of V_d. Attractively, our **PHI-6F/ZrO_2** and **PHI-BC/ZrO_2** hybrid systems do not only raise the RI effectively, but also upgrade V_d more efficiently than the respective TiO_2 hybrid systems. Furthermore, the advanced values of the RI-tunable **PHIs/ZrO_2** optical hybrid films for optical applications are having higher V_d and transparency than those of **PHIs/TiO_2** systems.

Characteristics and switching behaviors of the memory devices

UV-vis absorption spectra of the **PHIs** are shown in Fig. S6 (ESI†), and the energy band gap (E_g) can be estimated by the onset wavelength of optical absorption. Cyclic voltammetry (CV)

Table 2 Thermal properties of **PHIs** and **PHI** hybrid films with TiO_2 and ZrO_2

			Reactant composition/wt%		Hybrid film inorganic content/wt%		$T_d^{5\,d}$ (°C)		$T_d^{10\,d}$ (°C)		
Index	T_g^{a} (°C)	CTE^{b} (ppm °C^{-1})	Polymer	$Ti(OBu)_4/Zr(OBu)_4$	Theoretical	Experimental^{c}	N_2	Air	N_2	Air	R_{w800}^{e}/%
PHI-6F	350	73	100	0	0	0	450	430	500	490	30.6
PHI-BC	320	43	100	0	0	0	400	400	415	420	23.6
PHI-6FTi10	375	45	67.8	32.2	10	10.5	410	410	480	455	37.4
PHI-6FTi30	400	33	35.4	64.6	30	30.9	405	410	475	450	45.0
PHI-6FTi50	—	—	19.0	81.0	50	47.8	400	390	465	430	67.2
PHI-BCTi30	350	28	35.4	64.6	30	28.3	410	425	435	450	34.1
PHI-6FZr10	370	41	74.3	25.7	10	11.3	410	450	485	500	37.3
PHI-6FZr30	410	25	42.8	57.2	30	31.8	400	400	480	450	44.7
PHI-6FZr50	—	—	24.3	75.7	50	47.2	380	370	450	420	65.6
PHI-BCZr30	355	23	42.8	57.2	30	31.7	410	400	440	440	34.2

^{a} Glass transition temperature measured by TMA at a heating rate of 10 °C min^{-1} with a constant applied load of 5 mN by tension mode. ^{b} CTE data was determined over a 50–300 °C range by tension mode. ^{c} Experimental inorganic contents were calculated from TGA curves. ^{d} Residual weight percentages at 800 °C under nitrogen flow. ^{e} Temperature at which 5% and 10% weight loss occurs, reported by TGA at a heating rate of 20 °C min^{-1} and a gas flow rate of 30 cm^3 min^{-1}.

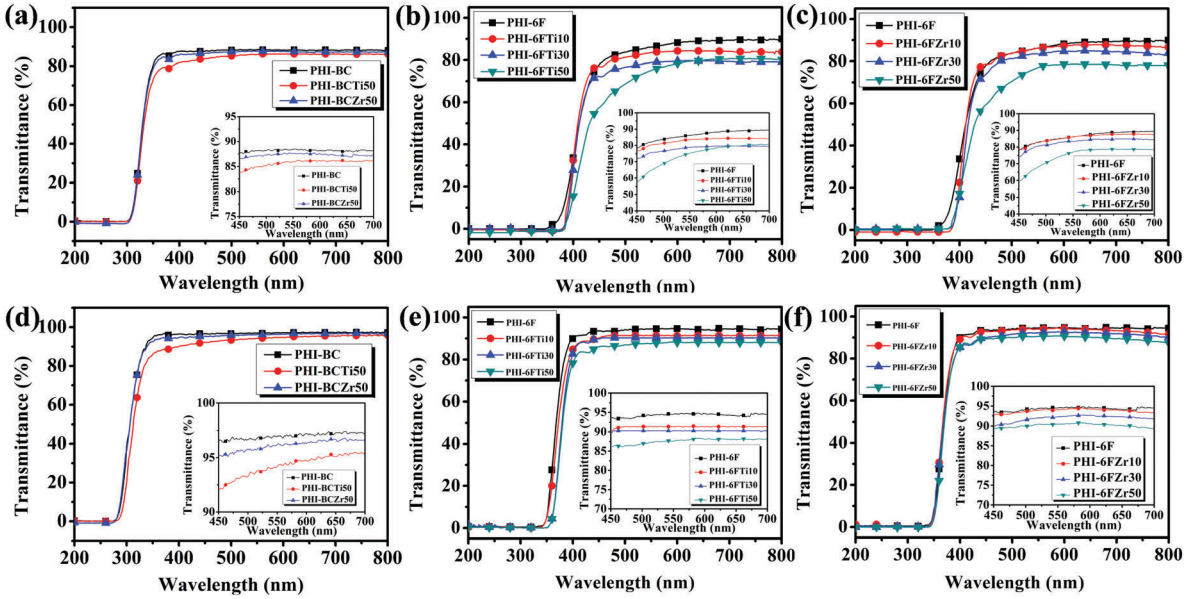

Fig. 2 Optical transmission spectra of **PHI-BCM50**, **PHI-6FTiX** and **PHI-6FZrX**: (a–c) thick hybrid films (thickness: 20 ± 5 μm); and (d–f) thin hybrid films (thickness: 200–300 nm). The inset figure displays the transmission spectra of thick and thin hybrid films in the wavelength range from 450 to 700 nm.

Table 3 Optical properties of **PHIs**, **PHI-6F** and **PHI-BC** hybrid films with TiO_2 and ZrO_2

	λ_0[a] (nm)	T_{400}[b] (%)	T_{450}[b] (%)	n[c]	Δn[d]	V_d[e]
PHI-6F	360/340	35/90	78/93	1.626	0.0060	24.26
PHI-BC	305/278	87/96	88/97	1.603	0.0063	26.39
PHI-6FTi10	380/342	22/84	77/90	1.690	0.0076	23.96
PHI-6FTi30	381/343	16/82	72/88	1.753	0.0094	24.45
PHI-6FTi50	381/344	15/78	56/86	1.839	0.0108	23.86
PHI-BCTi50	306/284	81/90	83/92	1.813	0.0112	26.38
PHI-6FZr10	384/342	32/88	78/92	1.668	0.0078	31.45
PHI-6FZr30	384/342	28/85	74/89	1.729	0.0097	33.31
PHI-6FZr50	386/344	18/84	58/87	1.813	0.0113	37.13
PHI-BCZr50	305/280	85/95	87/96	1.805	0.0118	36.77

[a] The cut-off wavelength (λ_0) from UV-vis transmission spectra of thick/thin polymer films (thickness: 20 ± 3 μm/200–300 nm). [b] Transmittance of thick/thin polymer films (thickness: 20 ± 3 μm/200–300 nm) at 400 nm and 450 nm. [c] Refractive index at 633 nm measured by ellipsometer. [d] The in-plane/out-of-plane birefringence (Δn) calculated with $\Delta n = n_{TE} - n_{TM}$ using a prism coupler. [e] Abbe's number is calculated by $V_d = n_{587.56} - 1/n_{486.1} - n_{656.3}$.

was used to obtain electrochemical characteristics of the **PHIs** under nitrogen atmosphere, employing 0.1 M tetrabutylammonium perchlorate (TBAP) as the electrolyte. The CV diagrams of **PHIs** are displayed in Fig. S7 (ESI†), and energy levels of HOMO can be calculated by the onset oxidation. In Table 4, the redox potentials of **PHIs** and the corresponding energy values of LUMO and HOMO are summarized. The memory properties of **PHIs** were evaluated by current–voltage (*I–V*) curves during the potential sweep of an Al/polymer/ITO sandwich-shaped device, and Al and ITO were used as the electrodes for applying voltage, which is shown in Scheme 4. The thickness of polymer films was set at 50 nm to eliminate the thickness effect on memory behaviour.[12]

For better understanding the **PHI**'s memory behaviour, the simulation of a molecular basic unit using the Gaussian 09 program was accomplished by DFT/B3LYP/6-31G(d). The experimental values in Table 4 were affirmative with the LUMO and HOMO energy levels derived from molecular simulation, and the isosurface charge density of basic units are also summed up in Fig. 5.

Fig. 6a and b exhibit *I–V* curves of the **PHI-6F**; the devices were retained only in the OFF state without switching to the ON state in positive sweeps up to 6 V with a current ranging from 10^{-13} to 10^{-15} A. A dramatic increase in current at −4.6 V during negative sweep with about 50% probability was observed, indicating an electrical transition between the OFF state and the ON state (writing process). Then, the device could remain in the ON state by continuous negative (the third sweep) and positive scans (the fourth sweep), and **PHI-6F** memory device did not return to the initial OFF state with an opposite electric field, implying non-erasable behaviour. After shutting the power down for about 10 s, the fifth sweep was operated, and it demonstrated that the relaxation from the ON state to the initial OFF state occurred, and the device could be switched to the ON state at −4.0 V again. Hence, DRAM characteristics of rewriting capability and short retention time are what the device owns. On the contrary, the device derived from **PHI-BC** could only be retained in the OFF state with a current ranging from 10^{-13} to 10^{-15} A, which is observed from the *I–V* curves as shown in Fig. 6c, without switching to the ON state both in positive and negative sweeps reaching 6 V and −6 V, correspondingly, denoting non-memory characteristics. According to previous reports,[12,13] the electrons at the LUMO (ON state) energy level will be first transmitted from the HOMO level when the applied electric field compasses the voltage causing accumulation of energy in the HOMO energy level and then assemble the

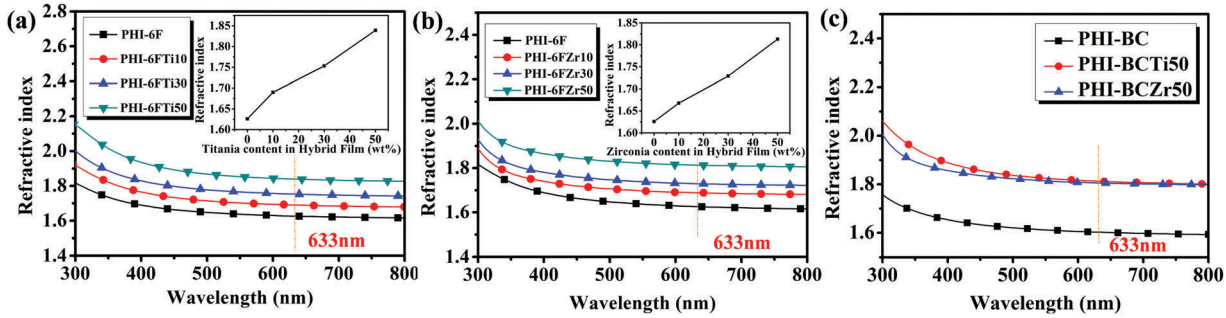

Fig. 3 Variation of the refractive index with wavelength of (a) **PHI-6FTiX**, (b) **PHI-6FZrX** and (c) **PHI-BCM50** hybrid films. The inset figure shows the variation of refractive index at 633 nm with different contents of titania and zirconia.

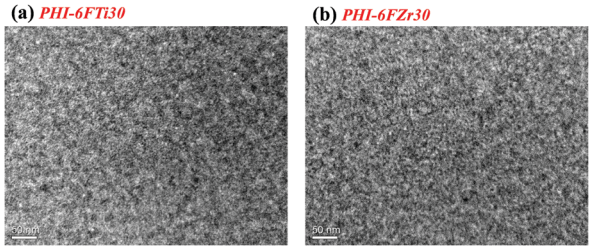

Fig. 4 TEM image of the (a) **PHI-6FTi30** and (b) **PHI-6FZr30** hybrid material.

Table 4 Redox potentials and energy levels of **PHIs**

Polymer	UV-vis absorption (nm) λ_{onset}	Oxidation potential[a] (V) E_{onset}	E_g[b] (eV)	HOMO[c] (eV)	LUMO (eV)
PHI-6F	327	0.81	3.79	−5.25	−1.46
PHI-BC	304	0.80	4.08	−5.24	−1.16

[a] The data were compared with Ag/AgCl in CH_3CN. [b] The data were calculated from polymer films using the following equation: $E_g = 1240/\lambda_{onset}$ (energy band gap between LUMO and HOMO). [c] The HOMO energy levels were calculated from CV and were referenced to ferrocene (4.8 eV; onset = 0.36 V).

charge-transfer complex *via* different ways that can switch the device to the ON state. The memory devices of **PHIs** exhibited distinct characteristics between **PHI-6F** and **PHI-BC** due to the different electron-withdrawing strengths of acceptor groups as shown in Fig. 5, 7a and b. The electron-withdrawing capability

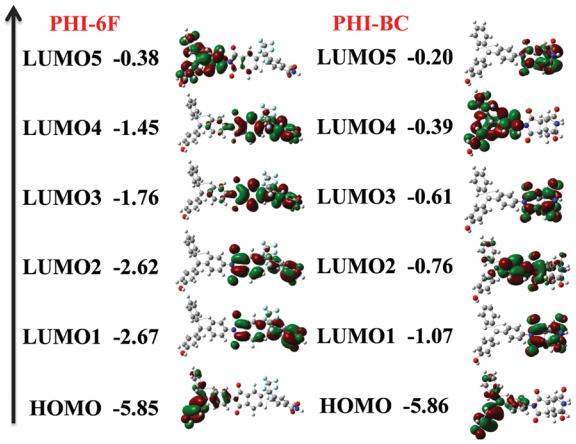

Fig. 5 Calculated molecular orbitals and the respective energy levels of basic units for **PHIs**.

of aromatic dianhydride with hexafluoroisopropylene (6F) group is stronger than that of the alicyclic dianhydride. Therefore, the memory device based on **PHI-6F** exhibited 50% none and 50% DRAM characteristics because that **PHI-6F** has better charge separation than **PHI-BC** and the charge transfer complex could be formed and stabilized which is shown in Fig. 5.

Furthermore, as electron acceptors, TiO_2 and ZrO_2 are introduced in PI hybrids to prepare memory devices, for which *I–V* curves are displayed in Fig. 8 and 9, respectively.

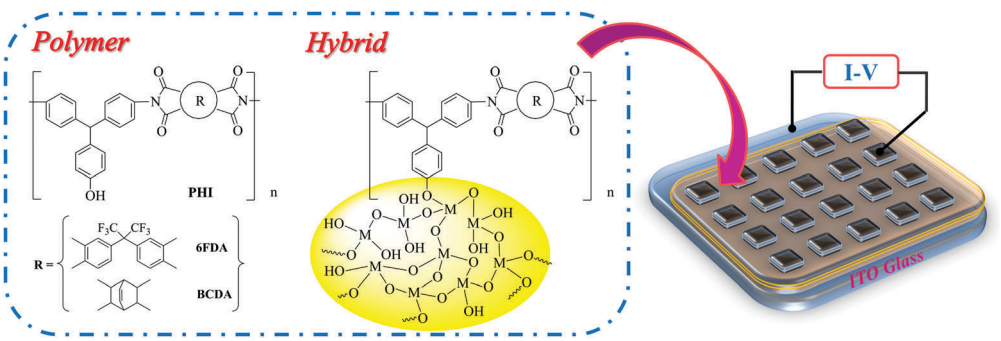

Scheme 4 Chemical structures of **PHIs**, **PHI-6F/TiO$_2$** and **PHI-6F/ZrO$_2$** and the structure of a memory device composed of a thin polymer film, which appears like a sandwich between an Al top electrode and an ITO bottom electrode.

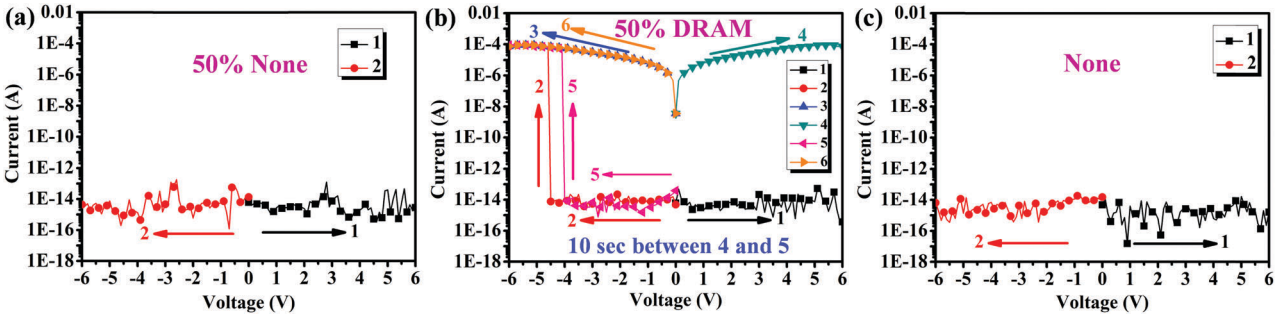

Fig. 6 Current–voltage (*I–V*) properties of the ITO/**PHIs** (50 ± 3 nm)/Al memory device (a), (b) **PHI-6F** and (c) **PHI-BC**.

The *I–V* curves of **PHI-6FTi5** hybrid with 5 wt% content of TiO_2 are shown in Fig. 8a and b, the device is maintained in the OFF state with a current ranging from 10^{-13} to 10^{-15} A without switching to the ON state in positive sweeps up to 6 V. A dramatic increase in the current at −4.4 V during negative sweep with about 80% probability can be observed, which indicates an electrical transition between the OFF state and the ON state (writing process); then, the device can remain in the ON state by continuous negative (the third sweep) and positive (the fourth sweep) scans. In addition, **PHI-6FTi5** memory devices did not return to the initial OFF state by an opposite electric field, indicating non-erasable behavior. After shutting down the applied voltage for about 25 s, the fifth sweep was operated, and it demonstrated that the relaxation from the ON state to the initial OFF state occurred, and the device switched to the ON state at −3.8 V again. Hence, the device reveals the DRAM characteristics of rewriting capability and short retention time.

The memory devices of **PHI-6FTi7** hybrid, containing 7 wt% content of TiO_2, switched from 10^{-15} to 10^{-4} A at −4.2 V threshold voltage in the negative sweep and then read the ON state by continuous negative (the third sweep) and positive (the fourth sweep) scans, which are displayed in Fig. 8c. Without the applied voltage, it returned to the OFF state from the ON state within 12 min, and then switched to the ON state at a threshold voltage of −3.6 V again, denoting a volatile SRAM-like behaviour.

The memory devices of **PHI-6FTi10** hybrids, containing 10 wt% content of TiO_2, switched from 10^{-15} to 10^{-4} A at a threshold voltage of −4.0 V in the negative sweep and then could read the ON state by following negative (the third sweep) and positive (the fourth sweep) scans, as depicted in Fig. 8d. After turning off the applied voltage, it returned to the OFF state from the ON state within 30 min, and then could be switched to the ON state at −3.4 V again as a volatile SRAM behaviour. To compare with volatile behaviour of SRAM and DRAM, the ON state of **PHI-6FTi15** with 15 wt% content of TiO_2 can be preserved even after shutting down the applied voltage for more than 2 h. Hence, the *I–V* curves of the memory device based on **PHI-6FTi15** film in Fig. 8e exhibited non-volatile WORM memory property, which is an abbreviation of write-once-read-many times. In addition, the devices prepared from **PHI-6FTi30** hybrids with 30 wt% content of TiO_2 revealed bi-switchable WORM characteristics at an applied voltage around 3.4 V summed up in Fig. 8f and g, respectively, because the energy band gap between LUMO of TiO_2 and ITO work function is smaller (Fig. 7c). Moreover, the stability in both the ON and OFF states of WORM memory devices prepared by **PHI-6FTi30** films is displayed in Fig. S8 (ESI†).

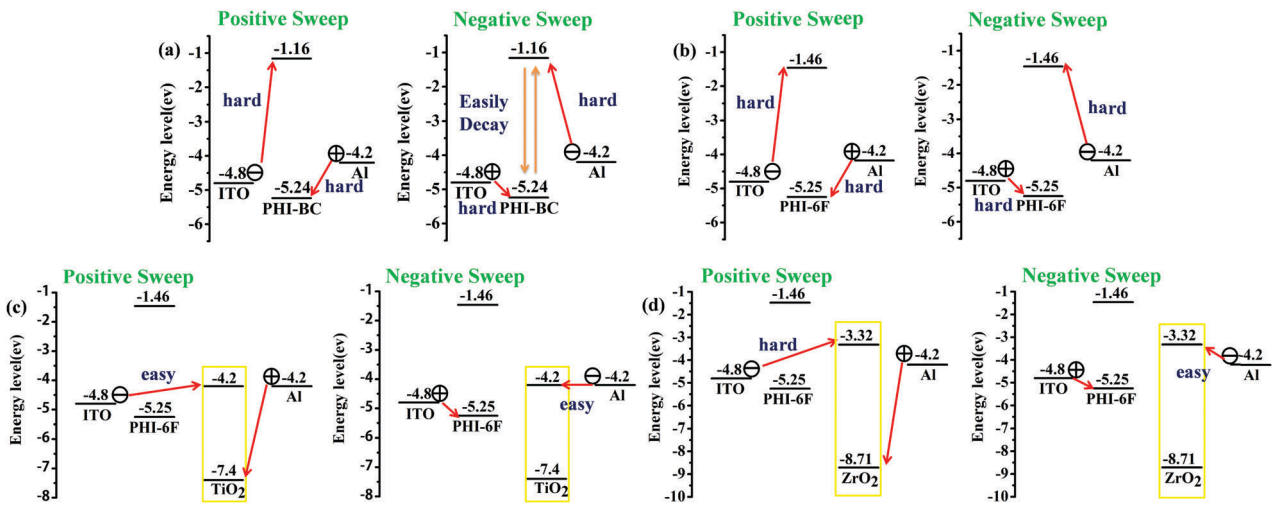

Fig. 7 HOMO and LUMO energy levels of (a) **PHI-BC**, (b) **PHI-6F** (c) **PHI-6F** and **TiO_2**, and (d) **PHI-6F** and **ZrO_2** along with work function of the electrodes.

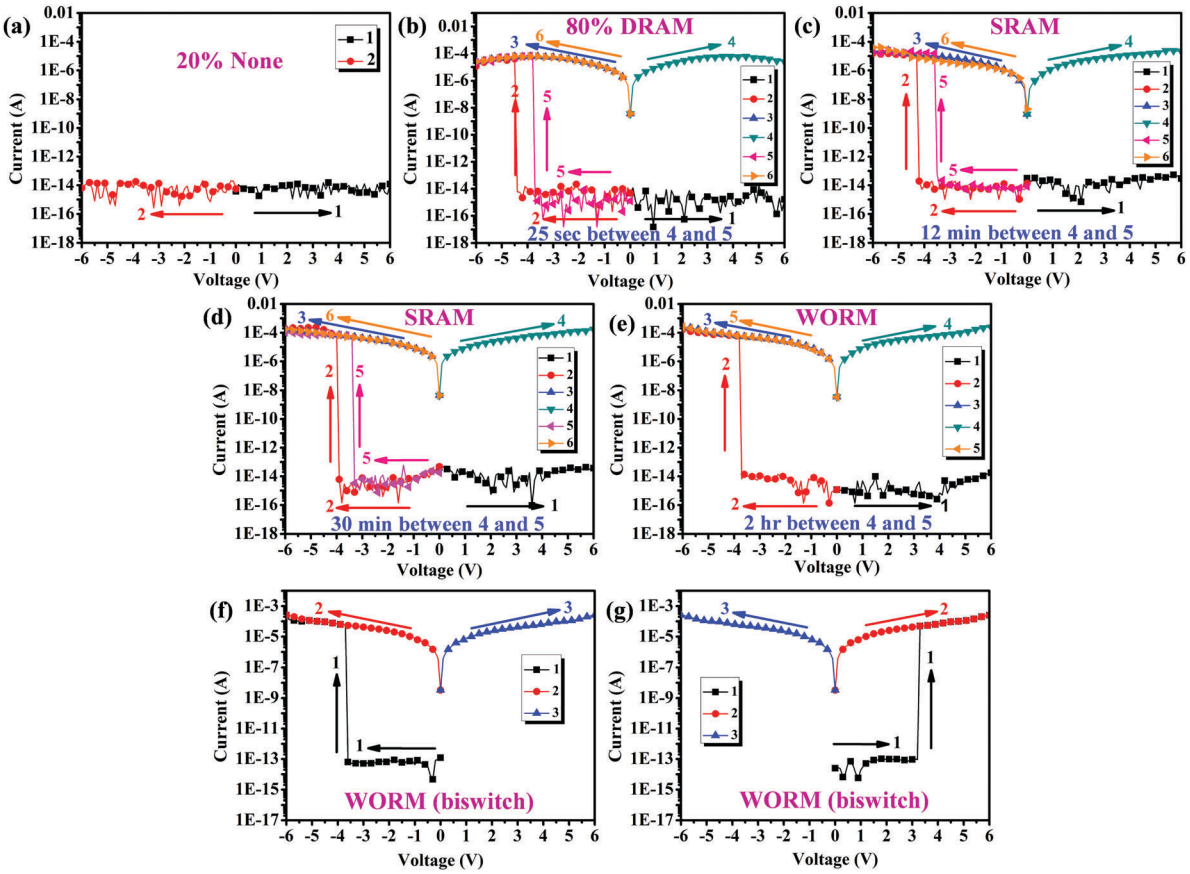

Fig. 8 Current–voltage (I–V) characteristics of the ITO/**PHI-6F/TiO_2** hybrid materials (50 ± 3 nm)/Al memory device (a and b) **PHI-6FTi5**, (c) **PHI-6FTi7**, (d) **PHI-6FTi10**, (e) **PHI-6FTi15**, and (f and g) **PHI-6FTi30**.

In addition, in order to demonstrate how inorganic materials affect the memory properties, the corresponding memory devices based on **PHI-6F/ZrO_2** hybrids were also fabricated for comparison, and results summed up in Fig. 9 display a memory behavior

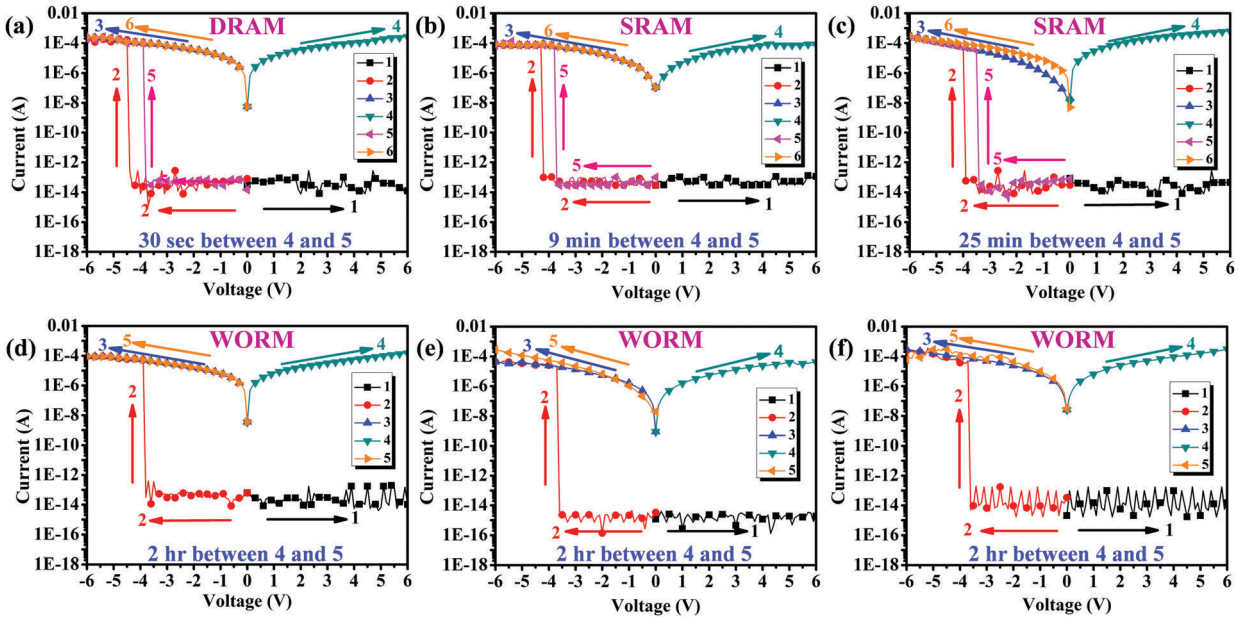

Fig. 9 Current–voltage (I–V) properties of the ITO/**PHI-6F/ZrO_2** hybrid materials (50 ± 3 nm)/Al memory device (a) **PHI-6FZr5**, (b) **PHI-6FZr7**, (c) **PHI-6FZr10**, (d) **PHI-6FZr15**, (e) **PHI-6FZr30** and (f) **PHI-6FZr50**.

Table 5 Summary of **PHI-6F**, **PHI-6F/TiO_2** and **PHI-6F/ZrO_2** memory properties

PHI-6F + TiO_2/ZrO_2	0 wt%	5 wt%	7 wt%	10 wt%	15 wt%	30 wt%	50 wt%
TiO_2 Memory Properties	50% none 50% DRAM (10 s)	20% none 80% DRAM (25 s)	SRAM (12 min)	SRAM (30 min)	WORM	WORM (bi-switch)	WORM (bi-switch)
ZrO_2 Memory Properties	50% none 50% DRAM (10 s)	DRAM (30 s)	SRAM (9 min)	SRAM (25 min)	WORM	WORM	WORM

almost the same to that of **PHI-6F/TiO_2** hybrids and also have extremely high ON/OFF current ratio (10^8). These memory devices of the **PHI-6F/ZrO_2** hybrid system reveal the same trend that the longer retention and lower threshold voltage can be achieved by increasing the content of ZrO_2.

Interestingly, the devices derived from **PHI-6F/ZrO_2** hybrids with a sufficiently high ZrO_2 content up to 50 wt% can just have mono-switchable and non-volatile WORM memory properties, which are displayed in Fig. 9f. This result is distinct to the bi-switchable characteristic from the respective **PHI-6FTi30** that can be attributed to higher LUMO energy levels of ZrO_2 than TiO_2, resulting in larger energy gap related to the work function of ITO as displayed in Fig. 7c and d. Thus, the obtained **PHI** hybrid materials with TiO_2 and ZrO_2 as electron acceptors have lower LUMO energy level that makes the CT complex stabilized and facilitated. As summarized in Table 5, the resulting hybrid devices manifested tunable memory behaviours from DRAM and SRAM, to WORM by varying the contents of ZrO_2 and TiO_2 ranging from 0 to 50 wt%. Overall, the difference in LUMO energy levels between TiO_2 and ZrO_2 results in uniquely distinct memory behaviour in terms of bi-switchable characteristics. Thus, the interesting and attractive results summarized in this study demonstrate that the prepared **PHIs/titania** and **PHIs/zirconia** hybrid films with high transparency have specific potential in the memory device applications.

Conclusions

Highly transparent and flexible polyhydroxyimides (**PHIs**) were successfully prepared by one-step polycondensation. The hydroxyl groups in the PHI backbones effectively contribute the reaction sites for the bonding between organic and inorganic materials, resulting in transparent and homogeneous films of the hybrid. These polymer hybrid films demonstrate extreme thermal stability associated with high T_g (350–410 °C) and low CTE (23 ppm $°C^{-1}$ for **PHI-BCZr30**). The transparency of **PHI-BC** thin films reaches 96% at 400 nm and RI of 1.63 for **PHI-6F** can be obtained. In addition, these polymer hybrid films show a tunable RI (1.63–1.84 for **PHI-6F/TiO_2** and 1.63–1.81 for **PHI-6F/ZrO_2**); the optical transparency and Abbe's number of **PHI-BC/ZrO_2** hybrids are higher than those of **PHI-BC/TiO_2** hybrids because of larger band gap of ZrO_2, which are tremendously valuable benefits for optical applications. Moreover, the obtained **PHI** hybrid materials with titania and zirconia as electron acceptors have lower LUMO energy levels that make the CT complex stabilized and facilitated. Consequently, the fabricated memory devices from these hybrid materials revealed impressive and tunable memory behaviours with an extremely high ON/OFF current ratio (10^8) by adjusting the titania or zirconia content from 0 to 50 wt%. Interestingly, the difference in LUMO energy levels between ZrO_2 and TiO_2 can result in distinct WORM-type memory devices (bi-switchable WORM for **PHI-6FTi30** and mono-switchable WORM for **PHI-6FZr30**).

Acknowledgements

The authors gratefully acknowledge the Ministry of Science and Technology of Taiwan for the financial support.

Notes and references

1 (*a*) L. L. Beecroft and C. K. Ober, *Chem. Mater.*, 1997, **9**, 1302; (*b*) C. Sanchez, F. Ribot and B. Lebeau, *J. Mater. Chem.*, 1999, **9**, 35; (*c*) G. Schottner, *Chem. Mater.*, 2001, **13**, 3422; (*d*) J. Pyun and K. Matyjaszewski, *Chem. Mater.*, 2001, **13**, 3436; (*e*) H. Schmidt, *Appl. Organomet. Chem.*, 2001, **15**, 331.

2 D. W. Mosley, K. Auld, D. Conner, J. Gregory, X. Q. Liu, A. Pedicini, D. Thorsen, M. Wills, G. Khanarian and E. S. Simon, *Proc. SPIE*, 2008, **6910**, 691017.

3 C. A. Terraza, J. G. Liu, Y. Nakamura, Y. Shibasaki, S. Ando and M. Ueda, *J. Polym. Sci., Part A: Polym. Chem.*, 2008, **46**, 1510.

4 (*a*) W. Groh and A. Zimmerman, *Macromolecules*, 1991, **24**, 6660; (*b*) K. Han, K. You, W. H. Jang and T. H. Rhee, *Macromol. Chem. Phys.*, 2000, **201**, 747; (*c*) J. L. Yan, Z. Wang, L. X. Gao and M. X. Ding, *Macromolecules*, 2006, **39**, 7555; (*d*) Y. Liu, Y. Xing, Y. H. Zhang, S. W. Guan, H. B. Zhang and Y. Wang, *J. Polym. Sci., Part A: Polym. Chem.*, 2010, **48**, 3281; (*e*) C. A. Terraza, J. G. Liu, Y. Nakamura, Y. Shibasaki, S. Ando and M. Ueda, *J. Polym. Sci., Part A: Polym. Chem.*, 2007, **46**, 1510.

5 (*a*) T. T. Suzuki, *Macromol. Mater. Eng.*, 2008, **293**, 109; (*b*) M. M. Demir, M. Memesa, P. Castignolles and G. Wegner, *Macromol. Rapid Commun.*, 2006, **27**, 763; (*c*) H. Cui, M. Zayat, P. G. Parejo and D. Levy, *Adv. Mater.*, 2008, **20**, 65.

6 (*a*) G. S. Liou, P. H. Lin, H. J. Yen, Y. Y. Yu, T. W. Tsai and W. C. Chen, *J. Mater. Chem.*, 2010, **20**, 531; (*b*) C. L. Tsai, H. J. Yen, W. C. Chen and G. S. Liou, *J. Mater. Chem.*, 2012, **22**, 17236; (*c*) H. J. Yen, C. L. Tsai, P. H. Wang, J. J. Lin and G. S. Liou, *RSC Adv.*, 2013, **3**, 17048; (*d*) C. L. Tsai, C. J. Chen, P. H. Wang, J. J. Lin and G. S. Liou, *Polym. Chem.*, 2013, **4**, 4570; (*e*) C. J. Chen, C. L. Tsai and G. S. Liou, *J. Mater.*

Chem., 2014, **2**, 2842; (*f*) C. L. Tsai and G. S. Liou, *Chem. Commun.*, 2015, **51**, 13523.

7 (*a*) H. W. Su and W. C. Chen, *J. Mater. Chem.*, 2008, **18**, 1139; (*b*) R. Himmelhuber, P. Gangopadhyay, R. A. Norwood, D. A. Loy and N. Peyghambarian, *Opt. Mater. Express*, 2011, **1**, 252.

8 H. Althues, J. Henle and S. Kaskel, *Chem. Soc. Rev.*, 2007, **36**, 1454.

9 (*a*) J. Ouyang, C. W. Chu, C. R. Szmanda, L. Ma and Y. Yang, *Nat. Mater.*, 2004, **3**, 918; (*b*) C. W. Chu, J. Ouyang, J. H. Tseng and Y. Yang, *Adv. Mater.*, 2005, **17**, 1440.

10 (*a*) C. J. Chen, C. L. Tsai and G. S. Liou, *J. Mater. Chem.*, 2014, **2**, 2842; (*b*) C. J. Chen, J. H. Wu and G. S. Liou, *Chem. Commun.*, 2014, **50**, 4335.

11 T. Nakayama, A. Mochizuki and M. Ueda, *React. Funct. Polym.*, 1996, **30**, 109.

12 C. J. Chen, Y. C. Hu and G. S. Liou, *Polym. Chem.*, 2013, **4**, 4162.

13 Q. D. Ling, F. C. Chang, Y. Song, C. X. Zhu, D. J. Liaw, D. S. H. Chan, E. T. Kang and K. G. Neoh, *J. Am. Chem. Soc.*, 2006, **128**, 8732.